APPLIED SCIENCES AND ENGINEERING

Self-powered electro-tactile system for virtual tactile experiences

Yuxiang Shi[1,2]*, Fan Wang[1,2]*, Jingwen Tian[1,2], Shuyao Li[1,2], Engang Fu[3], Jinhui Nie[1,2], Rui Lei[1], Yafei Ding[1,2], Xiangyu Chen[1,2]†, Zhong Lin Wang[1,2,4]†

Copyright © 2021 The Authors, some rights reserved; exclusive licensee American Association for the Advancement of Science. No claim to original U.S. Government Works. Distributed under a Creative Commons Attribution NonCommercial License 4.0 (CC BY-NC).

Tactile sensation plays important roles in virtual reality and augmented reality systems. Here, a self-powered, painless, and highly sensitive electro-tactile (ET) system for achieving virtual tactile experiences is proposed on the basis of triboelectric nanogenerator (TENG) and ET interface formed of ball-shaped electrode array. Electrostatic discharge triggered by TENG can induce notable ET stimulation, while controlled distance between the ET electrodes and human skin can regulate the induced discharge current. The ion bombardment technique has been used to enhance the electrification capability of triboelectric polymer. Accordingly, TENG with a contact area of 4 cm^2 is capable of triggering discharge, leading to a compact system. In this skin-integrated ET interface, touching position and motion trace on the TENG surface can be precisely reproduced on skin. This TENG-based ET system can work for many fields, including virtual tactile displays, Braille instruction, intelligent protective suits, or even nerve stimulation.

INTRODUCTION

Virtual reality (VR) and augmented reality (AR) are revolutionary technologies, aiming at creating virtual environments that allow human to obtain various feelings almost like real experiences in the physical world (*1*, *2*). Compared with the simulated feelings of sight, hearing, and smell, virtual tactile sense is much more difficult to be realized because it requires a fast-response, high-resolution, bio-friendly, and large-sized tactile stimulation technique, while it is the crucial element for distinguishing VR/AR system from other immersive video techniques (*3*, *4*). There are two major approaches for realizing artificial tactile sense, via mechanical or electrical stimulation. By applying localized mechanical force or vibration on skin, mechano-tactile devices can achieve safe and highly controllable stimulations for VR/AR sensation (*5*–*7*). However, this kind of VR/AR device is usually fabricated with complex structures and needs relatively high-power consumptions (*8*). Alternatively, electro-tactile (ET) devices are advantageous due to its small size, light weight, and high resolution (*9*–*12*). Nevertheless, the human epidermis has rather large resistances, which makes it quite challenging to decide an appropriate voltage for creating desired stimulations without pain (*13*, *14*). It is possible to lower down voltage and current value for electrostimulation by using needle electrodes to release signal under the epidermis, but this kind of penetration mode still has the risk of skin lesions and infections (*15*–*18*).

On the other hand, triboelectric nanogenerator (TENG) is a newly developed micro-energy technique with many unique characteristics (*19*–*22*), which may offer a different approach for traditional ET technique. Previously, TENG has been applied as a sensory device in VR/AR system. For example, Lee's group (*23*–*26*) has reported human-machine interfaces for VR applications based on this kind of self-powered sensors. However, the advantages of TENG for virtual tactile stimulations have not been fully explored. The ultrahigh electrostatic field provided by TENG is enough to stimulate skin through microgap discharge without direct contact or penetration (*27*–*29*). The output charge from TENG is a fixed value regulated by interfacial design (*30*–*33*), and these triboinduced charges exhaust very quickly during the discharging process (*34*), leading to a self-protection mechanism against electrical damage. Thus, it is possible to precisely control the induced current signal on skin for avoiding pains. Moreover, TENG can convert ambient and irregular mechanical energy into electricity (*35*–*37*). The ET arrays integrated with TENG have the potential to achieve a self-powered and wireless virtual tactile system, where immersed experience can be brought to people with no need of power supply.

Here, we propose a self-powered and skin-integrated ET system for realizing enhanced virtual tactile experiences. This ET system consisted of a TENG array and skin-integrated ET interface fabricated with ball-shaped electrode array integrated on the skin. The high output voltage and low output current of TENG can provide notable noncontact electrostimulation to skin, indicating a different approach for the field of virtual tactile sensations. By controlling the separation distance between electrode and human skin, this TENG-based ET system can precisely regulate the induced current on the skin, and a highly sensitive but painless virtual tactile experience is achieved. Meanwhile, ion bombardment technique has been applied to modify the electrification capability of triboelectric polymers, and the minimum size of TENG for triggering ET stimulation is achieved to be 4 cm^2, which can facilitate the integration process of an ET system on the human body. For perspective, this self-powered ET system can be integrated on a spacesuit or a positive-pressure protective suite to offer users a sensation of virtual physical contact with the outside. The proposed ET system will provide a new direction for TENG's application and extend self-powered virtual tactile stimulations to medical and aerospace fields.

[1]CAS Center for Excellence in Nanoscience, Beijing Key Laboratory of Micro-nano Energy and Sensor, Beijing Institute of Nanoenergy and Nanosystems, Chinese Academy of Sciences, Beijing 100083, China. [2]School of Nanoscience and Technology, University of Chinese Academy of Sciences, Beijing 100049, China. [3]State Key Laboratory of Nuclear Physics and Technology, Department of Technical Physics, School of Physics, Peking University, Beijing 100871, China. [4]School of Materials Science and Engineering, Georgia Institute of Technology, Atlanta, GA 30332-0245, USA.
*These authors contributed equally to this work.
†Corresponding author. Email: chenxiangyu@binn.cas.cn (X.C.); zhong.wang@mse.gatech.edu (Z.L.W.)

Downloaded from http://advances.sciencemag.org/ on February 3, 2021

RESULTS

Enhanced virtual tactile experiences enabled by TENG

A skin-integrated ET system is designed on the basis of an ET stimulating interface and a TENG array. Figure 1A depicts the working principle and operation process of the proposed ET system. The touching and sliding motion on TENGs can be directly transferred into electrostatic signals, while these signals are conducted to the ET interface integrated on human skin. Each ball-shaped electrode on the ET interface is connected with the specific TENG unit in the TENG array, and the signal provided by the TENG unit can induce electrostatic discharge from the ball-shaped electrode to the skin. Last, the virtual tactile stimulations with specific patterns are reproduced on skin through these electric stimulations. Figure 1B presents the disassemble structure of the ET interface and electrode array, where 21 ball-shaped electrodes are encapsulated in a wearable band. The tiny balls made of tin are 0.5 mm in diameter, and the distance between two adjacent electrodes is 15 mm. All the tin balls are conglutinated to copper (Cu) electrodes on one side of the polyethylene terephthalate (PET), which forms the discharging electrodes, and wires are arranged on the other side through prepared aperture. To avoid charge leakage and interference, both sides are packaged by dielectric polytetrafluoroethylene (PTFE). Last, a very high bonding (VHB) tape with designed thickness is applied to cover the ET interface, creating an adhesive surface for attaching on the skin. Figure 1C gives the discharging mechanism of the ET interface, where the TENG array of the sliding mode is used to provide driving power. A series of tiny holes are pouched on the VHB tape by laser drilling, and the ball-shaped electrodes can induce discharge signal through these holes (see Fig. 1C). As illustrated in fig. S1, the TENG array consists of a PTFE film (negative tribolayer) covering an array of back electrode (Cu), and a freestanding acrylic substrate covered by positive tribolayer for sliding motion. Each TENG unit is 20 × 20 mm, and the center-to-center distance of two adjacent units is 40 mm. The PTFE film is attached on the Cu electrodes as a negative tribolayer, to provide a smooth surface and to reduce the possible charge leakage through air. Previously reported ET devices usually rely on the pulse current transmitted from anode/cathode to ground electrode through the skin, in which two electrodes and the high electric current are indispensable (*10*, *16*). Moreover, the direct contact of skin with electrodes, whether it is shaped in pin or microneedle, can increase the risk of skin tearing and cause infections (*15*). In our case, the discharging electrode is working in noncontact mode, and the induced current is precisely controlled by TENG, which substantially reduces the risk of skin damage. In this ET interface, the controlled distance between the ball-shaped electrodes and the skin is regulated by the thickness of the elastic VHP tape (see fig. S2, A and B). It is worth mentioning that the current of discharge, especially powered by TENG, is much smaller than that of the reported ET display [5 mA of the ET device (*10*) and 0.96 to 1.83 mA of the ET tattoo (*14*)], contributing to safe stimulation to skin (under 10 mA) (*13*) as well as the simplification of the two-electrode mode to one-electrode fabrication. With the real-time output from TENGs and corresponding discharge stimulation, this ET interface can successfully reproduce virtual spatial patterns (e.g., figures and letters) to users.

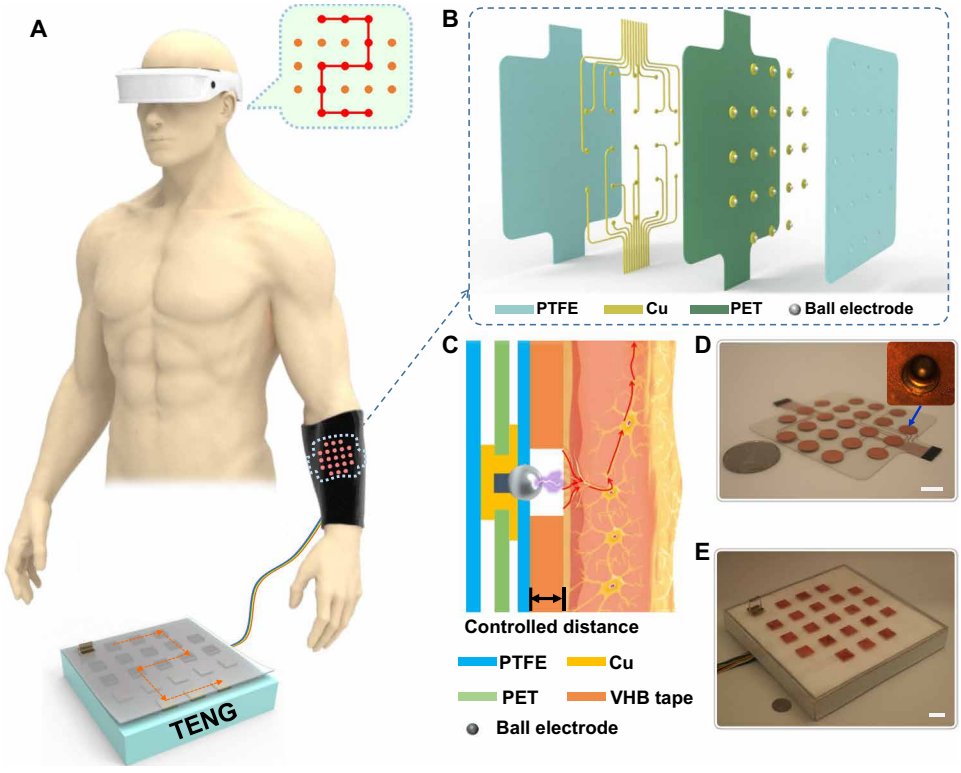

Fig. 1. Skin-integrated ET interface. (**A**) Schematic illustration of the ET system to transmit virtual spatial pattern. (**B**) Exploded view of the electrode array. (**C**) ET sense of the ET system (controlled distance, 0.4 mm). (**D**) Optical images of the electrode array (scale bar, 10 mm). The inset shows an enlarge view of a ball electrode (Φ = 0.5 mm). (**E**) Image of the TENG array (21 units sized in 20 × 20 mm; center-to-center distance, 40 mm; scale bar, 20 mm). Photo credit: Fan Wang, Chinese Academy of Sciences.

Downloaded from http://advances.sciencemag.org/ on February 3, 2021

The optical image of this electrode array is shown in Fig. 1D with an inset microscopic view of a ball-shaped electrode, and the optical image of TENG is displayed in Fig. 1E.

A sketch explaining the typical discharge stimulus powered by a TENG unit is illustrated in Fig. 2A. At the initial state (step I in Fig. 2A), PTFE and positive tribolayer are assumed to be fully charged, and equivalent positive charges are generated on the Cu surface because of electrostatic induction effect. When a positive tribolayer slides toward the PTFE, charges on Cu are driven away through the wire, and the charge accumulation on the ball-shaped electrode leads to a high potential difference between electrode and skin. When the positive tribolayer fully overlaps the PTFE in stage II, the potential difference between electrode and skin reaches the highest value. Thus, the discharge between the ball-shaped electrode and skin is induced, which results in an instantaneous electric current through skin to tactile nervous receptor and creates a sense of touch. In stage III, the continuous sliding of the positive tirbolayer causes a quite inverse potential difference and another discharge stimulation to skin. Figure S3 depicts the working process of the positive tirbolayer sliding across three positions above Cu electrodes, which can induce the related electrodes to discharge, respectively. Thus, the ET interface combined with TENG is able to instantly convert mechanical motions into ET stimulus in the form of discharge, indicating a bridge for people to experience virtual tactile communications.

The essential element of this ET system is a high-quality and long-term stable TENG device, while the output performance of the TENG device mainly depends on the material selection and surface treatment. In this ET interface, PTFE is selected as the negative triboelectric material because of its low price and high electrification performance after corona polarization (*38*). On the other hand, the ion bombardment technique has recently been used for modifying materials for capacitive energy storage (*39*), and we have also demonstrated that this technique can be used to improve the triboelectric performance of Kapton film (*32*). The ion bombarded Kapton with ion dose of $1 \times 10^{16}/cm^2$ shows very strong electron-donating capability during contact electrification (more positive than nylon and rubber). In this case, the similar ion bombardment technique has been applied to modify the TENG in this ET system. Moreover, in our previous study, ion irradiation cannot improve the PET film due to its weak thermostability (*32*). Hence, we apply polyethylene

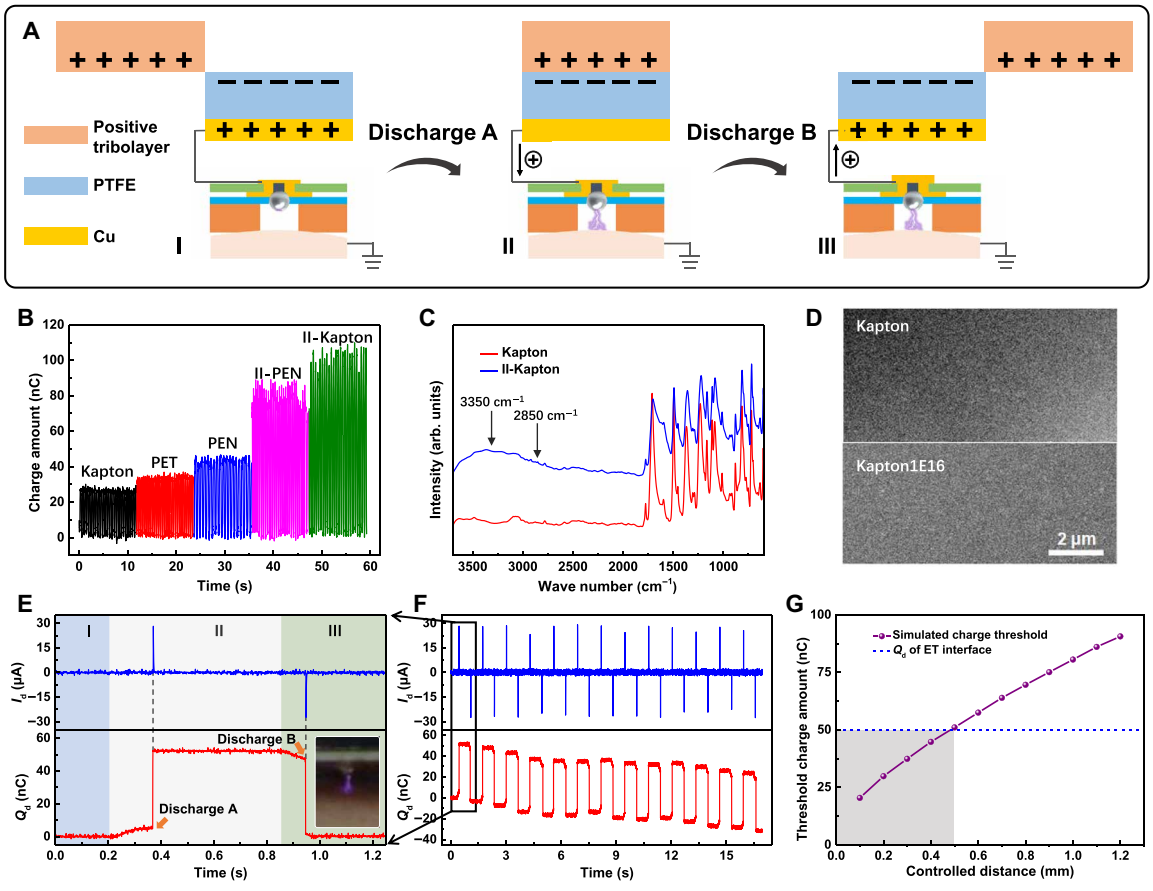

Fig. 2. Working mechanism and optimized electric outputs of ET interface. (**A**) Schematic diagram of ET stimulation powered by TENG. (**B**) Open-circuit transferred charge of friction between various positive tribomaterials [Kapton, PET, polyethylene naphthalate (PEN), ion-bombarded PEN (II-PEN), and ion-bombarded Kapton (II-Kapton)] with PTFE (effective tribo-area: 20 × 20 mm). (**C**) Attenuated total reflectance Fourier transform infrared (ATR-FTIR) spectra of the pristine Kapton film and II-Kapton (ion dose of $1 \times 10^{16}/cm^2$, 50 keV). arb. units, arbitrary units. (**D**) Scanning electron microscopy (SEM) images of Kapton and II-Kapton (scale bar, 2 μm). (**E**) Discharging current (I_d) and transferred charge (Q_d) in the process of (A) with an inset image of the discharge on skin (controlled distance, 0.5 mm; TENG sized 20 × 20 mm). (**F**) I_d and Q_d in numbers of friction circle. (**G**) Simulated charge threshold of ball-plate electrode under different controlled distances (air breakdown voltage, 30 kV/cm; ball electrode, Φ = 0.5 mm; and plate electrode, 0.1 × 10 mm). Photo credit: Yuxiang Shi, Chinese Academy of Sciences.

Downloaded from http://advances.sciencemag.org/ on February 3, 2021

naphthalate (PEN) with higher thermostability as an alternative this time. The output performances of these positive triboelectric materials [ion bombarded Kapton (II-Kapton), common Kapton, PET, PEN, and ion bombarded PEN (II-PEN)] with PTFE are compared with short-circuit transferred charges. First, the ion (He) dose of the bombardment is 1×10^{16} ions per cm^2 (50 keV), and the effective tribo-areas for the sliding-mode TENG is 20 × 20 mm. As is shown in Fig. 2B, the II-Kapton film exhibits the highest transferred charge amount (about 105 nC) during the triboelectrification, while the transferred charge amount of II-PEN (70 nC) is a bit lower than that of II-Kapton but higher than other materials, suggesting that ion bombardment is a helpful method to optimize the output performance of TENG. As a result, II-Kapton is selected as the positive triboelectric material in our experiments, to improve the compactness of the ET system for skin integration. Besides, considering that the humidity resistance of PEN is much higher than that of Kapton, which is an important characteristic when integrated on humid skin, the II-PEN is also a possible alternative for the ET system.

The increased electrification capabilities of II-Kapton and II-PEN are due to the change of chemical structure induced by ion bombardment. The related attenuated total reflectance Fourier transform infrared (ATR-FTIR) measurements have been performed. As shown in Fig. 2C and fig. S4A, the ATR-FTIR spectra of II-Kapton, an obvious new peak appears at around 3350 cm^{-1}, which is attributed to the breaking of the C—N bond (*40*, *41*) and the formation of new N—H bond. Another two peaks at 2920 and 2850 cm^{-1} appear simultaneously because of the generation of a carbonyl in the aldehyde group (—CHO), which proves that a C—H and an N—H bond are formed in the Kapton's molecular skeleton after bombardment. It means that a new group —NHCOR is established (fig. S4B). When combined with the benzene ring in the II-Kapton skeleton, the electron-donating ability of group —NHCOR is greatly enhanced due to the conjugation of the benzene ring. The combining effects make II-Kapton become a highly positive triboelectric material. The surface morphology of II-Kapton is also studied by scanning electron microscopy (SEM), and there are no substantially surface topography or roughness changes on the Kapton after ion bombarded (Fig. 2D). Similar results are also obtained in the ATR-FTIR spectra of PEN and II-PEN. As depicted in fig. S5 (A and B), the increased intensity at 3300 to 3600 cm^{-1} and a peak appearing at 2850 cm^{-1} in the spectrum of II-PEN result from the stretching vibration of O—H and C—H, which can prove that the ester group (—COO—) is broken (fig. S5C). The same result can also be found in ion bombarded PET (*42*). The O—H bond (terminal group) gives rise to the strong electron-donating ability of II-PEN, so the transferred charge amount increases obviously during the electrification. The SEM image of II-PEN shows slight changes in surface topography after ion bombardment (fig. S5D), which means the polymer chains are broken during the bombardment progress. This is derived from its weaker thermal stability than Kapton and also explains its lower transferred charge amount than II-Kapton. In fig. S5E, we have compared the output performance of different contact-pair materials, and the combination of PTFE and II-Kapton can provide the highest transferred charges under short-circuit conditions. The short-circuited transferred charge (Q_{sc}) of TENG composed of PTFE and II-Kapton (20 × 20 mm) is shown in fig. S6A, where the average Q_{sc} for each motion cycle is about 105 nC. For each stimulating unit on the ET interface, its ability to trigger discharge is qualified through the discharging current (I_d) and the related transferred charge (Q_d). The schematic measurement circuit of Q_d and I_d is exhibited in fig. S6B, where a Cu film (10 × 10 mm) as ground electrode is put to represent human skin and the ball-shaped electrode is 0.5 mm in diameter. Figure 2E illustrates a typical result of Q_d and I_d during the discharging process, where two step changes of Q_d (50 nC) and two peak currents of 25 μA can be both observed. As explained in Fig. 2A, two discharging currents are induced during the sliding motion, which are related to the position of fully overlapping (discharge A) and fully separating (discharge B), respectively. The inset in Fig. 2E shows an image of discharge on skin captured by a high-speed camera. It is worth mentioning that the Q_d of discharge B is nearly equal to that of discharge A (Fig. 2F), and the induced two peak currents have almost the same amplitude, which proves the charge conservation in this progress.

The discharge mechanism of ET interface on human skin

A theoretical ball-plate model has been established by COMSOL to simulate this discharge process. As shown in fig. S6C, a ball electrode (Φ = 0.5 mm) is suspended above a grounded plate electrode (0.1 × 10 mm), and the controlled distance is 0.5 mm. According to the air breakdown voltage (Paschen's law: 30 kV/cm under standard atmospheric pressure), the threshold voltage for discharging is around 1500 V. When the controlled distance increases to 1.0 mm (fig. S6D), the required threshold voltage and the charge amount on the ball electrode are 3000 V and 80.5 nC, respectively. The threshold charge amount (Q_{ET}) with various controlled distances between the ball electrode and the plate (from 0.1 to 1.2 mm) is depicted in Fig. 2G, where the dotted line (in blue) respects the Q_d in the real measurements (Fig. 2F). Hence, we can approximately estimate that the TENG (20 × 20 mm) is capable of driving discharge within a controlled distance of 0.5 mm (the region shadowed in gray).

According to a classical RC circuit of the electrostatic model and considering the internal capacitor of the TENG device (C_T), the self-powered ET system can be simplified into a circuit shown in fig. S7. The tribo-induced charge at short-circuited conditions (Q_{sc}: 105 nC) should be shared by C_T and the capacitor of ET interface (C_{ET}). The capacitance of C_{ET} on the ET interface is calculated as 34 pF by COMSOL (controlled distance of 0.5 mm), which is supposed to be comparable with the C_T of TENG. The related threshold charge amount for discharging is calculated to be 51 nC. As long as the charge amount reaches this threshold value, the discharge phenomenon can happen. Hence, the static charge accumulated on the ball-shaped electrode (Q_{ET}) is calculated as $Q_{ET} = Q_{sc} \times C_{ET}/(C_{ET} + C_T)$. Moreover, the C_{ET}' s voltage U_{ET} and the discharge current i can be calculated through this RC model

$$U_{ET}(t) = V_0 e^{-\frac{t}{RC_{ET}}} \quad (1)$$

$$i(t) = \frac{V_0}{R} e^{-\frac{t}{RC_{ET}}} \quad (2)$$

where V_0 is the initial output voltage of TENG and R is the discharge resistance in the fig. S7. The detail analysis process is demonstrated in note S1.

It is interesting to find that the high electrostatic field of TENG can trigger discharge effect even with ungrounded flat conductor. The detailed demonstration can be found in fig. S8A, where a Cu foil (40 × 40 mm) is fully isolated with substrate (acrylic) as an ungrounded electrode. The ball-shaped electrode powered by a TENG

Downloaded from http://advances.sciencemag.org/ on February 3, 2021

(20 × 20 mm) can still induce discharge current with this isolated Cu foil (under a controlled distance of 0.5 mm), as can be seen in fig. S8B. This phenomenon is caused by the screen effect of conductor in an electrostatic field, which leads to an internal electric field across the conductor. The electrostatic discharge with foils of different conductivity is shown in fig. S8C, and conductive rubbers made by mixing silicone rubber and carbon black are also prepared, where resistances can be regulated by the mixing ration of carbon black (fig. S8D). When the rubber's resistance increases to 15.38 megohms/cm, the discharge cannot be easily triggered. The skin resistance is much lower than this value, which shows no influence to the ET system (the inset image in Fig. 2E). Aiming to reveal the mechanism of electrostatic discharge with ungrounded electrode, a ball-plate model was established in fig. S9A. When 50-nC charges are accumulated on the ball electrode and the plate electrode is ungrounded (suspended), the potential difference between the controlled distance (0.5 mm) is calculated to be 1510 V (fig. S9B), which is enough for triggering discharge. However, when the plate electrode is removed (fig. S9C), the potential difference within 0.5 mm around the ball electrode is only 960 V (fig. S9D). Hence, fully isolated plate electrode and human body can be considered as an equipotential body, and the screening effect of equipotential body leads to the concentration of local electric field with this small gap, which also causes electrostatic discharge.

Currently, the skin stimulation devices based on batteries are mainly working with in-contact electrode (or needle electrodes). In this case, each stimulation unit should have two electrodes (an output electrode and a grounded electrode). Otherwise, a controllable current loop cannot be established. Alternatively, TENG combined with noncontact electrodes can produce notable electrical stimulation based on gap discharging. Thus, each stimulation unit of TENG only needs one electrode (the skin serves as the grounded electrode). Even if human body is isolated from the ground, the ET interface can still induce electrostatic discharge to the human skin and provide the virtual tactile sensations for humans under various conditions. Accordingly, the complexity of the electrode array with noncontact mode can be largely reduced, which helps to reduce the cost and improve the resolution of the ET interface.

On-skin ET interface and the tactile sensation

As illustrated in Fig. 3A, an on-skin ET interface with 21 stimulating units is prepared to demonstrate the capability of this self-powered ET technique for displaying complicated tactile information on human skin. The structure and the composition of this ET system are explained in Fig. 1, where the ET stimulating interface is connected to a TENG array, and sliding motion on TENGs can induce electrostatic signal on the ET interface. When the sliding substrate covered by II-Kapton film moves on the TENG surface from electrode (Cu) 2 to 20, a series of peak voltage signals are generated on the related electrodes (see Fig. 3B). The discharge current on the ET interface has been recorded as a superimposed graph in Fig. 3C, showing no interference to the electrodes outside the motion path. Consequently, a two-dimensional contour plot of the peak value of open-circuit voltage from all the electrode of TENG array is obtained in Fig. 3D, which explicitly reveals the moving path of II-Kapton. The high electrostatic field on the target electrode only slightly influences the surrounding electrodes, indicating this ET system owns high accuracy to realize a noninterfering ET stimulation.

Meanwhile, the structure parameters of the interface, including controlled distance, center-to-center distance, and the curvature of ball electrode, are important factors to guarantee a painless, sensitive, and noninterfering ET experience. As is shown in Fig. 3E, the transferred charge Q_d during discharging increases gradually with the increasing controlled distance, which means the discharge from the wider gap needs a larger amount of static charge. Accordingly, the discharge current is increased with the enlarged controlled distance, which may result in a painful ET sensation, and the discharge spark shows increasing brightness under width controlled distance (movie S1). It is important to note that the discharge current is mainly decided by controlled distance, and it is almost irrelevant to the size of TENG. If the size of TENG is too large, then it can induce multiple discharges within one motion cycle. Meanwhile, if the size of TENG is too small, then it cannot induce the discharge. To determine an appropriate controlled distance to realize a perceptible feeling without pain, 10 volunteers are recruited to test the pain degree induced by ET stimulation on their skin (forearm) under various controlled distance (1.5 to 0.2 mm). The statistical results are exhibited in fig. S10A. When the controlled distance is at 1.5 mm, all the participants feel pain. With the decrease in controlled distance, feedbacks of the painful feeling decrease gradually, and until controlled distance is at 0.5 to 0.4 mm, all participants feel perceptible stimulation without pain. When it comes to 0.3 mm, one participant starts to give feedback of imperceptibility, and about half of the participants feel imperceptible with a discharge induced at 0.2 mm. Thus, the optimal controlled distance is within 0.3 to 0.5 mm, and the VHB tape (with discharge tunnels on its surface) of 0.5 mm in thickness is applied to connect the ET interface and skin. Considering the deformation of human skin and VHB tape, the controlled distance of the ET system is supposed to be 0.3 to 0.5 mm (fig. S10B). It is important to note that some part of the skin may have large deformation during the daily motions. We have also designed another type of ET unit with sealed discharge channel for this kind of positions, which can precisely maintain the controlled distance for discharging. As shown in fig. S11 (A and B), two ball-shaped electrodes are located at the two ends of the discharging channel. Here, the channel should be fabricated with hard substrate, and the ball-shaped electrode on the bottom should be firmly stuck on the skin. In this case, the controlled distance in the channel can be precisely maintained, and the discharging current induced between two electrodes can also trigger a tactile feeling on the skin (fig. S11C), as shown in fig. S11 (D and E).

To determine a suitable center-to-center distance of the ball electrodes, a two-point discrimination experiment is proposed to study the spatial resolution of the ET system (controlled distance, 0.5). The statistical results of the two-point stimulus on the forearm are shown in fig. S12A, which clearly shows that 80% of participants are capable of recognizing 10 mm separated two-point stimulus on their forearm. Furthermore, the skin on the finger is much more sensitive than that on the forearm. We also prepare the discrimination experiment on human finger, as can be seen in fig. S12B. The average two-point discrimination threshold on the index finger is about 3 mm. These results indicate this ET system can realize a high spatial resolution on the human body. Furthermore, the diameter of the ball-shaped electrode also has impacts on the discharge, because the surface charge density is higher on a curved surface than on a plate. In this way, the amount of Q_d under the ball-shaped electrodes with different diameter is compared in Fig. 3F. When discharge is

Downloaded from http://advances.sciencemag.org/ on February 3, 2021

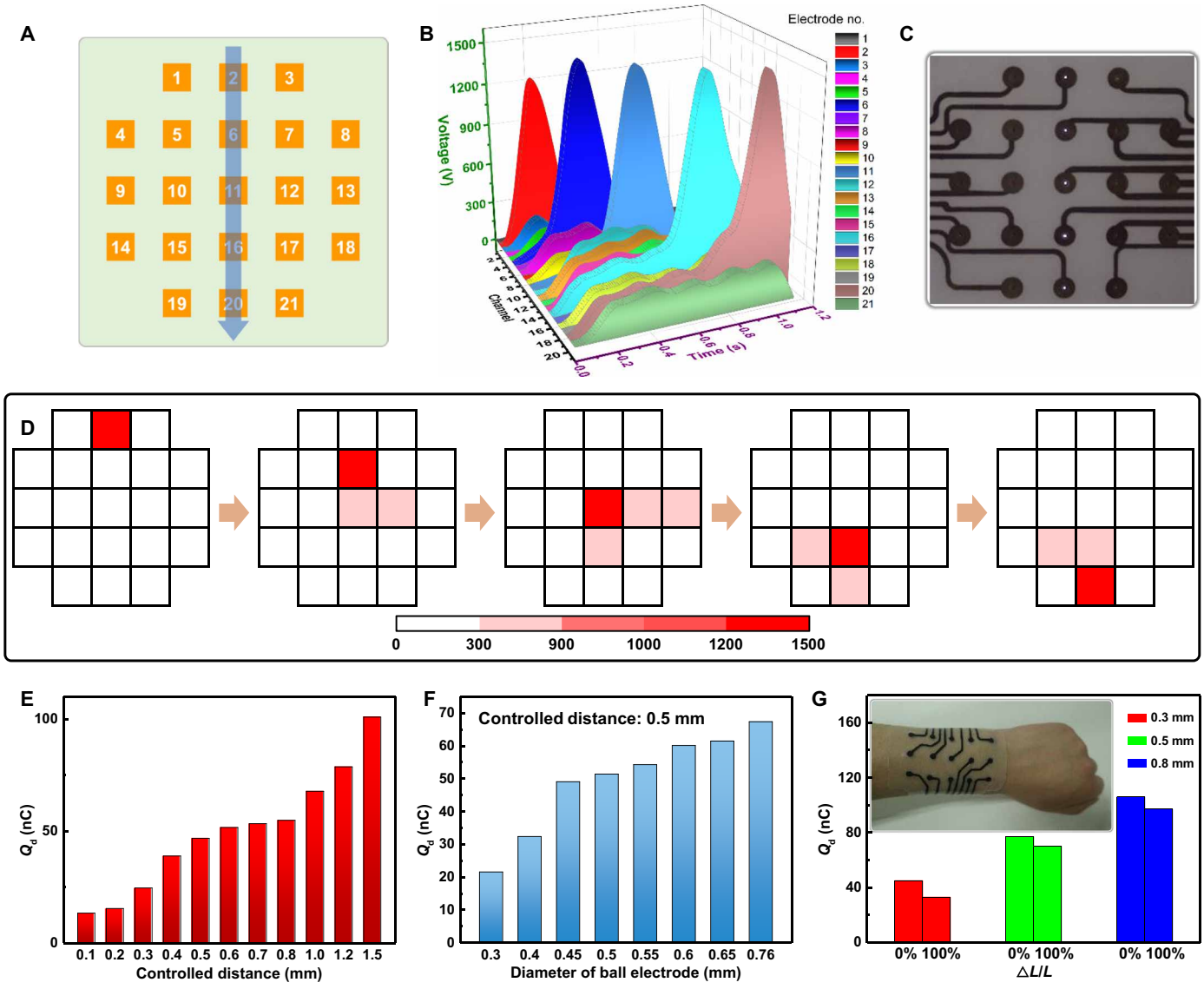

Fig. 3. Noninterference and influential factors test of ET interface. (**A**) Path of II-Kapton sliding from electrodes 2 to 21. (**B**) Open-circuit voltages of TENG array when II-Kapton moves from 2 to 21. (**C**) A superimposed image of the discharge induced by the sliding II-Kapton. (**D**) Mapping figures of open-circuit voltage when II-Kapton arrives at the center of an electrode. (**E**) Transferred charges (Q_d) of discharging at various controlled distances (0.1, 0.2, 0.3, 0.4, 0.5, 0.6, 0.7, 0.8, 1.0, 1.2, and 1.5 mm). (**F**) Amount of Q_d when discharging on ball electrode of different curvatures (0.15, 0.2, 0.225, 0.25, 0.25, 0.275, 0.3, 0.325, and 0.38 mm). (**G**) Q_d amount (discharging at controlled distance of 0.3, 0.5, and 0.8 mm) of the stretchable electrode when strained (0 and 100%). Photo credit: Yuxiang Shi, Chinese Academy of Sciences.

triggered at the same controlled distance (0.5 mm), a gradual increase in Q_d is observed with diameter changing from 0.3 to 0.76 mm, which suggests that discharge is easier to be induced under a smaller diameter. However, the ball-shaped electrode with very small diameter is not so easy to be assembled on the ET interface, and a medium diameter of 0.5 mm is selected for the ball-shaped electrode.

In view of the sweat secretion of human skin, the atmospheric humidity around the skin is a factor influencing discharge of ET interface. As studied in fig. S13A, the transferred charge during the discharging process is stable with humidity between 10 and 50%, and it decreases slightly when humidity reaches 70%. The atmospheric humidity around the skin surface in an enclosed space is collected by the method shown in fig. S13B, where the atmospheric humidity reaches a saturation value at about 65% after 6 min (fig. S13C), and the operation of the ET interface shows no influence under this humidity. As for the high skin humidity (100%) caused by excessive sweat, the influence of charge leakage cannot be neglected. In this case, the ET interface can be improved by adding a filmy cotton tissue between the VHB tape and the skin (fig. S13, D and E), which can help further absorb sweat. Furthermore, the discharging stability of the ET interface is also studied by measuring Q_d over 30-min repeated operation. As is shown in fig. S13F, the amount of Q_d shows some small fluctuations during the measurement, while it would not influence the reliability of the ET system.

Downloaded from http://advances.sciencemag.org/ on February 3, 2021

Aiming to improve the flexibility of the ET interface, another type of ET interface with good stretchability is fabricated with silicone rubber (the inset in Fig. 3G). The inner conductive electrode is obtained through mixing silicone rubber with carbon black and carbon nanotubes (CNTs). The relationship between resistance and tensile strain of this electrode is shown in fig. S14A, and the inset gives an optical image of the flexible interface. The resistance of initial length (20 mm) is about 3.4 kilohms and increase to about 9.0 kilohms with 100% strain, while all these resistances is much smaller than the matching resistance of TENG. The controlled distance of this stretchable ET interface is restricted with a ring-shaped rubber (0.5 mm; fig. S14B), and Q_d under different controlled distances are compared in Fig. 3G between the pristine and the tensile (100%). The discharge current and Q_d at 0.5-mm controlled distance are displayed in fig. S14 (C and D). The discharge current is lower than that in Fig. 2F, which is possibly due to the energy loss caused by the high resistance.

After obtaining the minimized TENG and ET interface with optimized structure, the feedback testing is applied for this ET system, to demonstrate perceptible ET stimulation to human. As shown in movie S2, discharge with designed sequence can be induced on human skin with good repeatability. Furthermore, spatial patterns of letters and figures can be performed on the TENG surface, and the induced electrostatic signal can precisely reproduce the same motion patterns on the ET interface, which is visualized through discharge on an indium-tin-oxide (ITO) glass electrode (movie S3). Figure 4 summarizes a possible application of this ET system as a virtual interaction technique, where TENG can serve as a bridge for people at different places to experience virtual tactile communications. As shown in Fig. 4A, the ET interface is attached to the forearm of a girl, whose eyes are covered. On the basis of the ET stimulation induced by TENG, the girl is capable of giving right feedbacks when random numbers are being written on the surface of TENG, as can be seen in Fig. 4B and movie S4. Before the video demonstration, the girl has been practiced for several times with each number. As this ET system is able to transfer virtual signals into tactile sensations through ET stimulus, it is expected to combine auditor and visual stimuli to establish complete VR systems for enhancing tactile experiences during noncontact communications, such as an isolation ward or prison visiting. In addition, this ET system can also be applied for dynamic Braille display (fig. S15A), which may help blind people read changeable characters. As can be seen in fig. S15 (B and C), the ET system with six electrodes can produce different Braille characters (fig. S15D), while the writing motion on the TENG surface can produce both the information and the stimulation energy.

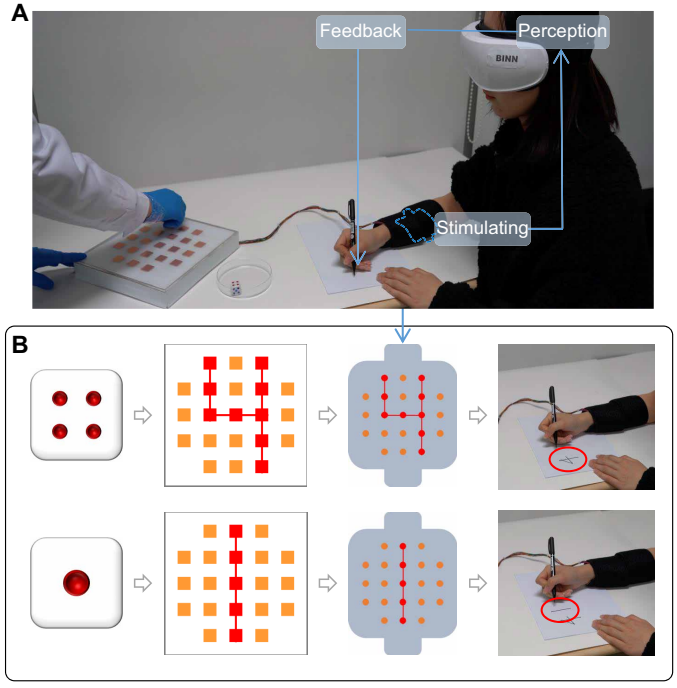

Fig. 4. An example of ET interface applied for enhancing tactile VR experience of precepting virtual spatial patterns (random figures). (**A**) Image when a girl facilitated with ET interface is accepting the test. (**B**) Schematic diagram of the test including generating random figure, imputing signaling through TENG array, ET stimulating by wearable electrode array, and giving feedback. Photo credit: Jingwen Tian, Chinese Academy of Sciences.

Fully integrated ET system for augmented tactile sensations

There are certain circumstances where people's tactile sensation is weakened or blocked, such as wearing armor, protective suits, or even space suits. Therefore, an integrated ET system based on contact separation TENG is designed to enhance tactile sensations for these application scenarios. Figure 5A exhibits the basic structure of this fully integrated ET system on an acrylic shell, where a contact separation TENG composed of PTFE and II-Kapton as triboelectric materials is set on the outer side of the substrate (acrylic). The effective contact area of this TENG unit is around 35 × 40 mm, and the output voltage is generated on the Cu electrode beneath the II-Kapton film. The ball-shaped electrode for ET discharging is attached on the other side with wires linking to the Cu electrode, and a block of sponge (area of 25 × 25 mm, 10 mm in thickness) is sandwiched between the discharging electrode and acrylic shell as a cushion, to guarantee the close contact. Besides, the controlled distance (0.3 to 05 mm) is also fixed with the VHB tape. This ET system can be attached on human forearm to mimic the situation of wearing a protective suit, where the sponge cushions and ball-shaped electrodes are closely attached on human skin. Then, the touching or the impact motion on the TENG outside the acrylic shell can trigger ET effect on the forearm inside the acrylic shell, leading to an AR tactile experience. As shown in Fig. 5B and fig. S16A, 16 ET units can be assembled on a semicylinder substrate (Φ = 90 mm, L = 200 mm) and 28 units on a cylinder (fig. S16B). Figure 5C displays the ET system integrated on the forearm and then encapsulated by cloth. The detailed working principle of this ET system is illustrated in fig. S16C. Similar to the explanation in Fig. 2A, PTFE and II-Kapton film are charge saturated at the initial stage. When the PTFE film moves toward the II-Kapton film (stage I to stage II), the induced charges accumulate on the ball-shaped electrode and generate a discharging effect. After PTFE is released (stage III), the TENG produces a reverse voltage signal, followed by another discharging. The discharge current (controlled distance, 0.5 mm) of an ET unit is measured in Fig. 5D, which is about 25 μA on average, and the transferred charge amount during discharging is around 44 nC (Fig. 5E). Furthermore, the discharge current at different controlled distances (0.5, 0.4, and 0.3 mm) driven by the same TENG unit is shown in movie S5. As shown in Fig. 5F, the proposed ET system

Downloaded from http://advances.sciencemag.org/ on February 3, 2021

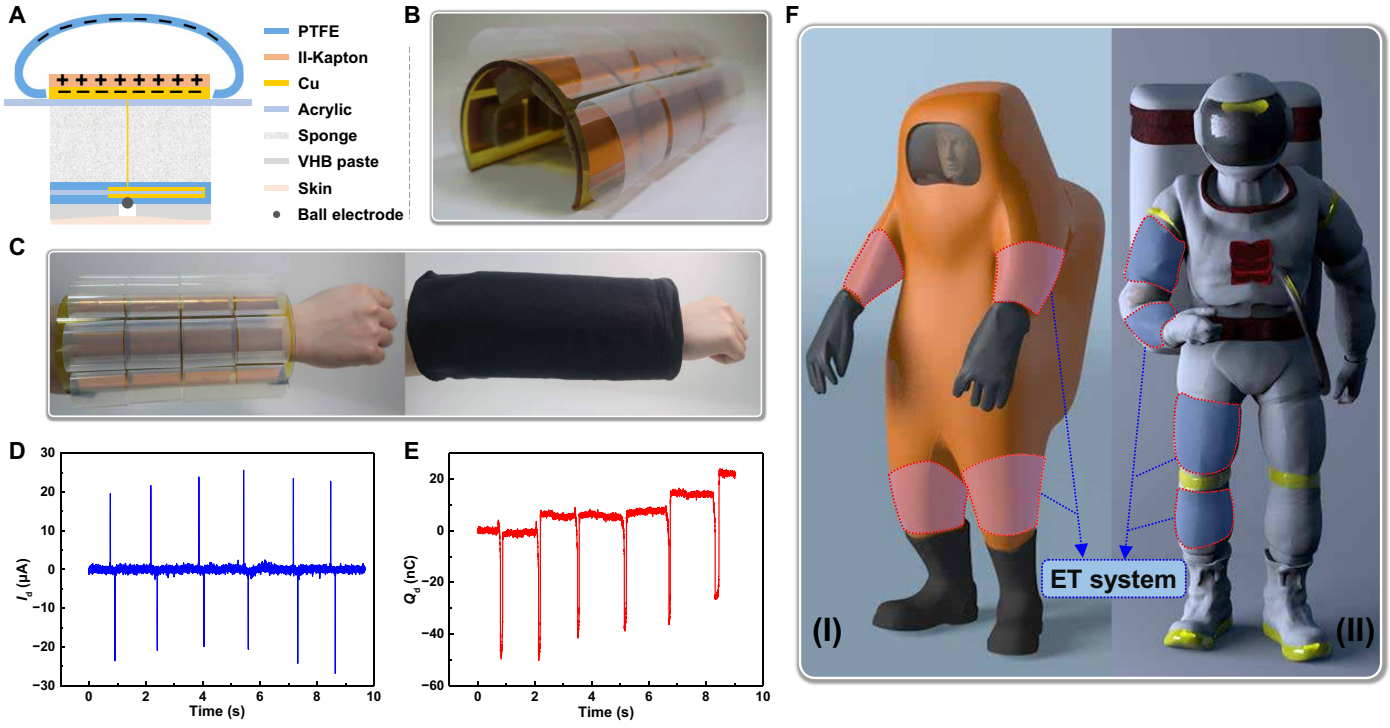

Fig. 5. An integrated ET system. (**A** to **C**) The structure of an ET unit (A), optical image of the system fabricated in semicylinder (B), and illustration when integrated on forearm (C). (**D** and **E**) The discharging current (D) and transferred charges (E) of the ET system unit. (**F**) Schematic diagram of positive-pressure protective suit (I) and spacesuit (II) equipped with the ET system (the shaded location), respectively. Photo credit: Jingwen Tian, Chinese Academy of Sciences.

can be integrated with various smart protective cloths, such as positive-pressure suits for biological and chemical protection [Fig. 5F (I)] or space suits for astronauts [Fig. 5F (II)]. With these protective suits, human tactile sensations of surrounding environments are strongly weakened, and accordingly, potential damage to the protective suit on the blind area of the user may not be easily and timely noticed. By applying this kind of ET system, it is possible to achieve an intelligent protective suit, where the users can obtain a more sensitive interaction with the surrounding environment. Moreover, this TENG-based ET system has the advantage of simple structure, low cost, and zero-power consumption, showing great applicability with different protective suits. Hence, this self-powered ET system can be integrated on various locations [shaded in Fig. 5F (I) and (II)] and provide a series of information about contact or hurt to the user through enhanced tactile sensation (fig. S16D). The similar system can also be applied on artificial limb (fig. S17), which can help the user learn more information during the operation of the artificial limb.

DISCUSSION

A skin integrated ET system has been proposed with the help of the TENG technique, which can provide harmless, sensitive, and zero-power virtual tactile experiences. The high voltage of TENG can trigger noncontact electrostatic discharge as stimulation, and the limited triboelectric charges of TENG can maintain the induced current on the skin to be lower than 25 μA, leading to a notable and painless tactile sensation. To minimize the TENG units, low-energy ion bombardment is applied as a surface modification method to enhance the surface charge density of TENG. Hence, TENG of size 20 × 20 mm is capable of triggering discharge under controlled distance of 0.5 mm, indicating a compact system for integration. A spatial resolution of 3 mm on human finger and 10 mm on the forearm is achieved through this ET interface. For mechanism analysis, we find that this kind of microgap discharge can be induced by the screen effect of the human body. Even if the human body or the discharging electrodes are fully suspended from the ground, this ET system can still provide ET stimulation. An on-skin ET matrix with 21 stimulating points is fabricated to demonstrate virtual tactile sensation, where both the touching position and the motion trace on a remote TENG array can be precisely reproduced on human skin through ET stimulus. Last, a wearable and wireless ET system based on TENG array is integrated on the human forearm, to demonstrate the possible application of this ET system for smart protective suits. This fully integrated and self-powered ET system can provide augmented tactile sensations for the users inside the suits and help them establish real-time virtual contact with the physical world. This TENG-based ET system is the first demonstration of a self-powered virtual tactile stimulation system, indicating a different approach for solving the sustainability problem and wire restriction of traditional VR/AR technique. Hence, it can promote the application of tactile VR/AR in many fields, including but not limited to tactile prosthetics, Braille instruction, intelligent protective suits, and so on.

MATERIALS AND METHODS

Test of the pain degree and two-point threshold

Ten participants (six males and four females) aged 22 to 35 were arranged in the test. The experiment of pain degree was conducted

Downloaded from http://advances.sciencemag.org/ on February 3, 2021

using an electrode shown movie S1. Each participant was instructed to give the pain degree [imperceptible, perceptible (no pain), slightly painful, and painful] of stimulation when discharge was induced on their skin (forearm) for three times under various controlled distances (1.5, 1.2, 1.0, 0.8, 0.7, 0.6, 0.5, 0.4, 0.3, and 0.2 mm).

In the test of two-point threshold, the two-point stimuli (controlled distance, 0.5 mm) were a set of six distances on the index finger (1.0, 0.7, 0.5, 0.4, 0.3, and 0.2 mm) and forearm (3.0, 2.5, 2.0, 1.5, 1.0, and 0.5 mm), respectively. Participants were asked to discriminate whether the stimulus is one or two after discharge was induced for three times. If the participant was able to discriminate two points correctly at a given distance, then the test was continued until getting the smallest distance.

Fabrication of the flexible electrode array

First, the inner electrode was obtained by adding the mixture of conductive carbon black and CNTs (2:1, weight ratio) into a breaker, and mixing with the base and cure (volume ratio: 1: 1) of the silicone rubber (Ecoflex 00-30). The mass ratio of the two mixtures was 1:13. After being stirred uniformly, the mixture was coated over a piece of acrylic, treated under 30°C for 5 hours, and, lastly, obtained a piece of conductive carbon black/CNTs@silicone rubber. Then, it was cut in the shape shown in Fig. 3G (the inset image) to obtain the stretchable electrode. The electrode was encapsulated with pristine silicone rubber and experienced another curing process under 30°C for 5 hours. Last, the ball electrode was stuck to the conductive rubber through a prepared hole, and after the ring-shaped rubber was pasted, the flexible electrode array was obtained.

Ion bombardment

Before radiation exposure, the pristine Kapton and PEN (20 × 20 mm) are adhered to the same area of aluminum. The ions are bombarded onto the polymer's surface at room temperature using an NEC 400-kV ion implanter. All experiments are performed with 50-keV He ions. The applied ion beam potential is 50 kV, and the bombardment dose is controlled to be 1×10^{16} ions/cm^2. The projected range value calculated by the Monte Carlo–based program Stopping and Range of Ions in Matter is less than 600 nm.

Materials

Four polymer films for TENG, including PTFE (80 μm in thickness), Kapton (55 μm in thickness), PET (50 μm in thickness), PEN (50 μm in thickness), and tin ball of various diameters (0.3, 0.4, 0.45, 0.5, 0.55, 0.6, 0.65, and 0.76 mm) were available in the market without further modification. The VHB tape used for controlling the distance between the ET interface and human skin is a kind of acrylic elastomer (0.5 mm thick, VHB MRO-S10, 3M).

Characterization and measurements

A programmable electrometer (Keithley 6514) was used to test the open-circuit transferred charge, discharge current, and resistance. A Trek 347 electrostatic voltmeter was used to measure the open-circuit voltage of TENG. An SEM (SU8020, Hitachi) was used to characterize the morphologies of the polymers. An FTIR spectroscope spectrometer (VERTEX80v, Bruker) was used to measure the ATR-FTIR spectrum. A commercial voltage source (ET2673A) was induced for comparing I_d powered by TENG.

Experiments with human subjects

We have studied the skin feeling of 10 different participants. The experiments with these human subjects have been performed in compliance with all the ethical regulations under a protocol that was approved by the Institutional Review Board at Beijing Institute of Nanoenergy and Nanosystems, Chinese Academy of Sciences. The participants are the authors of the paper and three other members in our laboratory (X. Tao, X. Wang, and Y. Lin). All of us gave written, informed consent about the experimental procedure.

SUPPLEMENTARY MATERIALS

Supplementary material for this article is available at http://advances.sciencemag.org/cgi/content/full/7/6/eabe2943/DC1

REFERENCES AND NOTES

1. D. Matthews, Virtual-reality applications give science a new dimension. *Nature* **557**, 127–128 (2018).
2. X. Yu, Z. Xie, Y. Yu, J. Lee, A. Vazquez-Guardado, H. Luan, J. Ruban, X. Ning, A. Akhtar, D. Li, B. Ji, Y. Liu, R. Sun, J. Cao, Q. Huo, Y. Zhong, C. M. Lee, S. Y. Kim, P. Gutruf, C. Zhang, Y. Xue, Q. Guo, A. Chempakasseril, P. Tian, W. Lu, J. Y. Jeong, Y. J. Yu, J. Cornman, C. S. Tan, B. H. Kim, K. H. Lee, X. Feng, Y. Huang, J. A. Rogers, Skin-integrated wireless haptic interfaces for virtual and augmented reality. *Nature* **575**, 473–479 (2019).
3. S. Sundaram, P. Kellnhofer, Y. Li, J.-Y. Zhu, A. Torralba, W. Matusik, Learning the signatures of the human grasp using a scalable tactile glove. *Nature* **569**, 698–702 (2019).
4. M. Zhu, Z. Sun, Z. Zhang, Q. Shi, T. He, H. Liu, T. Chen, C. Lee, Haptic-feedback smart glove as a creative human-machine interface (HMI) for virtual/augmented reality applications. *Sci. Adv.* **6**, eaaz8693 (2020).
5. S. Ryu, D. Pyo, S.-C. Lim, D.-S. Kwon, Mechanical vibration influences the perception of electrovibration. *Sci. Rep.* **8**, 4555 (2018).
6. H. A. Sonar, A. P. Gerratt, S. P. Lacour, J. Paik, Closed-loop haptic feedback control using a self-sensing soft pneumatic actuator skin. *Soft Robot.* **7**, 22–29 (2020).
7. S. Park, H. Kim, M. Vosgueritchian, S. Cheon, H. Kim, J. H. Koo, T. R. Kim, S. Lee, G. Schwartz, H. Chang, Z. Bao, Stretchable energy-harvesting tactile electronic skin capable of differentiating multiple mechanical stimuli modes. *Adv. Mater.* **26**, 7324–7332 (2014).
8. C. Fang, Y. Zhang, M. Dworman, C. Harrison, Wireality: Enabling complex tangible geometries in virtual reality with worn multi-string haptics, *In Proceedings of the 2020 CHI Conference on Human Factors in Computing Systems* (2020), pp. 1–20.
9. D. S. Pamungkas, K. Ward, Electro-tactile feedback system to enhance virtual reality experience. *Int. J. Comput. Theory Eng.* **8**, 465–470 (2016).
10. K. Sato, S. Tachi, Design of electrotactile stimulation to represent distribution of force vectors, *2010 IEEE Haptics Symposium* (Waltham, MA, 2010), pp. 121–128.
11. S. Parsnejad, Y. Gtat, R. Aridi, J. W. Brascamp, A. J. Mason, Inciting high fidelity tactile sensations using a single electrotactile electrode pair, *2019 9th International IEEE/EMBS Conference on Neural Engineering (NER)* (San Francisco, CA, USA, 2019), pp. 778–781.
12. M. S. Beauchamp, D. Oswalt, P. Sun, B. L. Foster, J. F. Magnotti, S. Niketeghad, N. Pouratian, W. H. Bosking, D. Yoshor, Dynamic stimulation of visual cortex produces form vision in sighted and blind humans. *Cell* **181**, 774–783.e5 (2020).
13. M. Kono, T. Takahashi, H. Nakamura, T. Miyaki, J. Rekimoto, Design guideline for developing safe systems that apply electricity to the human body. *ACM Trans. Comput. Hum. Interact.* **25**, 1–36 (2018).
14. A. Withana, D. Groeger, J. Steimle, Tacttoo: A thin and feel-through tattoo for on-skin tactile output, *Proceedings of the 31st Annual ACM Symposium on User Interface Software and Technology* (2018), pp. 365–378.
15. M. Tezuka, N. Kitamura, K. Tanaka, N. Miki, Presentation of various tactile sensations using micro-needle electrotactile display. *PLOS ONE* **11**, e0148410 (2016).
16. M. Tezuka, N. Kitamura, N. Miki, Micro-needle electro-tactile display, *28th IEEE International Conference on Micro Electro Mechanical Systems (MEMS)* (Estoril, 2015), pp. 5781–5784.
17. N. Kitamura, J. Chim, N. Miki, Micro-needle electrode array for electro tactile display, in *Transducers* (Barcelona, Spain, 2013), pp. 106–107.
18. M. Ortiz-Catalan, E. Mastinu, P. Sassu, O. Aszmann, R. Branemark, Self-contained neuromusculoskeletal arm prostheses. *N. Engl. J. Med.* **382**, 1732–1738 (2020).
19. F.-R. Fan, Z.-Q. Tian, Z. L. Wang, Flexible triboelectric generator. *Nano Energy* **1**, 328–334 (2012).
20. Z. L. Wang, Triboelectric nanogenerator (TENG)–sparking an energy and sensor revolution. *Adv. Energy Mater.* **10**, 2000137 (2020).
21. Z. L. Wang, J. Chen, L. Lin, Progress in triboelectric nanogenerators as a new energy technology and self-powered sensors. *Energ. Environ. Sci.* **8**, 2250–2282 (2015).

Downloaded from http://advances.sciencemag.org/ on February 3, 2021

22. R. Hinchet, H.-J. Yoon, H. Ryu, M.-K. Kim, E.-K. Choi, D.-S. Kim, S.-W. Kim, Transcutaneous ultrasound energy harvesting using capacitive triboelectric technology. *Science* **365**, 491–494 (2019).
23. Q. Shi, C. Lee, Self-powered bio-inspired spider-net-coding interface using single-electrode triboelectric nanogenerator. *Adv. Sci.* **6**, 1900617 (2019).
24. T. Chen, M. Zhao, Q. Shi, Z. Yang, H. Liu, L. Sun, J. Ouyang, C. Lee, Novel augmented reality interface using a self-powered triboelectric based virtual reality 3D-control sensor. *Nano Energy* **51**, 162–172 (2018).
25. Q. Shi, Z. Zhang, T. Chen, C. Lee, Minimalist and multi-functional human machine interface (HMI) using a flexible wearable triboelectric patch. *Nano Energy* **62**, 355–366 (2019).
26. J. Zhu, H. Wang, Z. Zhang, Z. Ren, Q. Shi, W. Liu, C. Lee, Continuous direct current by charge transportation for next-generation IoT and real-time virtual reality applications. *Nano Energy* **73**, 104760 (2020).
27. J. Nie, X. Chen, Z. L. Wang, Electrically responsive materials and devices directly driven by the high voltage of triboelectric nanogenerators. *Adv. Funct. Mater.* **29**, 1806351 (2018).
28. A. Li, Y. Zi, H. Guo, Z. L. Wang, F. M. Fernández, Triboelectric nanogenerators for sensitive nano-coulomb molecular mass spectrometry. *Nat. Nanotechnol.* **12**, 481–487 (2017).
29. J. Cheng, W. Ding, Y. Zi, Y. Lu, L. Ji, F. Liu, C. Wu, Z. L. Wang, Triboelectric microplasma powered by mechanical stimuli. *Nat. Commun.* **9**, 3733 (2018).
30. S. Li, J. Nie, Y. Shi, X. Tao, F. Wang, J. Tian, S. Lin, X. Chen, Z. L. Wang, Contributions of different functional groups to contact electrification of polymers. *Adv. Mater.* **32**, 2001307 (2020).
31. S. Wang, Y. Xie, S. Niu, L. Lin, C. Liu, Y. S. Zhou, Z. L. Wang, Maximum surface charge density for triboelectric nanogenerators achieved by ionized-air injection: Methodology and theoretical understanding. *Adv. Mater.* **26**, 6720–6728 (2014).
32. S. Li, Y. Fan, H. Chen, J. Nie, Y. Liang, X. Tao, J. Zhang, X. Chen, E. Fu, Z. L. Wang, Manipulating the triboelectric surface charge density of polymers by low-energy helium ion irradiation/implantation. *Energ. Environ. Sci.* **13**, 896–907 (2020).
33. S. Xu, Y. Wei, J. Liu, R. Yang, Z. L. Wang, Integrated multilayer nanogenerator fabricated using paired nanotip-to-nanowire brushes. *Nano Lett.* **8**, 4027–4032 (2008).
34. X. Xia, J. Fu, Y. Zi, A universal standardized method for output capability assessment of nanogenerators. *Nat. Commun.* **10**, 4428 (2019).
35. Y. Yang, H. Zhang, Z.-H. Lin, Y. S. Zhou, Q. Jing, Y. Su, J. Yang, J. Chen, C. Hu, Z. L. Wang, Human skin based triboelectric nanogenerators for harvesting biomechanical energy and as self-powered active tactile sensor system. *ACS Nano* **7**, 9213–9222 (2013).
36. J. Wang, S. Li, F. Yi, Y. Zi, J. Lin, X. Wang, Y. Xu, Z. L. Wang, Sustainably powering wearable electronics solely by biomechanical energy. *Nat. Commun.* **7**, 12744 (2016).
37. F. Wang, Z. Ren, J. Nie, J. Tian, Y. Ding, X. Chen, Self-powered sensor based on bionic antennae arrays and triboelectric nanogenerator for identifying noncontact motions. *Adv. Mater. Technol.* **5**, 1900789 (2020).
38. W. Du, J. Nie, Z. Ren, T. Jiang, L. Xu, S. Dong, L. Zheng, X. Chen, H. Li, Inflammation-free and gas-permeable on-skin triboelectric nanogenerator using soluble nanofibers. *Nano Energy* **51**, 260–269 (2018).
39. J. Kim, S. Saremi, M. Acharya, G. Velarde, E. Parsonnet, P. Donahue, A. Qualls, D. Garcia, L. W. Martin, Ultrahigh capacitive energy density in ion-bombarded relaxor ferroelectric films. *Science* **369**, 81–84 (2020).
40. B. D. Silverman, J. W. Bartha, J. G. Clabes, P. S. Ho, A. R. Rossi, Molecular orbital analysis of the XPS spectra of PMDA-ODA polymide and its polyamic acid precursor. *J. Polym. Sci. Part A Polym. Chem.* **24**, 3325–3333 (1986).
41. S. C. Park, S. S. Yoon, J. D. Nam, Surface characteristics and adhesive strengths of metal on O_2 ion beam treated polyimide substrate. *Thin Solid Films* **516**, 3028–3035 (2008).
42. Z. Zhu, Y. Sun, C. Liu, J. Liu, Y. Jin, Chemical modifications of polymer films induced by high energy heavy ions. *Nucl. Instr. Meth. B* **193**, 271–277 (2002).

Acknowledgments: We thank X. Tao, X. Wang, and Y. Lin as participants in testing the pain degree and two-point threshold. **Funding:** This work was supported by the National Key R&D Project from the Ministry of Science and Technology (2016YFA0202704), the National Natural Science Foundation of China (grant no. 51775049), the Beijing Natural Science Foundation (4192069), the Beijing Municipal Science and Technology Commission (Z171100000317001), the Young Top-Notch Talents Program of Beijing Excellent Talents Funding (2017000021223ZK03), and the Beijing Nova program (Z201100006820063). **Author contributions:** X.C. and Z.L.W. conceived the idea and supervised the experiment. Y.S., F.W., and J.T. prepared the manuscript. Y.S. and F.W. designed the structure of the device. Y.S. and F.W. performed the data measurements. S.L. and E.F. performed the ion bombardment treatment in the laboratory of Peking University. J.N., R.L., and Y.D. offered assistance with the experiments. All the authors discussed the results and commented on the manuscript. **Competing interests:** The authors declare that they have no competing interests. **Data and materials availability:** All data needed to evaluate the conclusions in the paper are present in the paper and/or the Supplementary Materials. Additional data related to this paper may be requested from the authors.

Submitted 12 August 2020
Accepted 16 December 2020
Published 3 February 2021
10.1126/sciadv.abe2943

Citation: Y. Shi, F. Wang, J. Tian, S. Li, E. Fu, J. Nie, R. Lei, Y. Ding, X. Chen, Z. L. Wang, Self-powered electro-tactile system for virtual tactile experiences. *Sci. Adv.* **7**, eabe2943 (2021).

Downloaded from http://advances.sciencemag.org/ on February 3, 2021

Science Advances

Self-powered electro-tactile system for virtual tactile experiences

Yuxiang Shi, Fan Wang, Jingwen Tian, Shuyao Li, Engang Fu, Jinhui Nie, Rui Lei, Yafei Ding, Xiangyu Chen and Zhong Lin Wang

Sci Adv **7** (6), eabe2943.
DOI: 10.1126/sciadv.abe2943

ARTICLE TOOLS http://advances.sciencemag.org/content/7/6/eabe2943

SUPPLEMENTARY MATERIALS http://advances.sciencemag.org/content/suppl/2021/02/01/7.6.eabe2943.DC1

REFERENCES This article cites 36 articles, 3 of which you can access for free
http://advances.sciencemag.org/content/7/6/eabe2943#BIBL

PERMISSIONS http://www.sciencemag.org/help/reprints-and-permissions

Use of this article is subject to the Terms of Service

Science Advances (ISSN 2375-2548) is published by the American Association for the Advancement of Science, 1200 New York Avenue NW, Washington, DC 20005. The title *Science Advances* is a registered trademark of AAAS.

Copyright © 2021 The Authors, some rights reserved; exclusive licensee American Association for the Advancement of Science. No claim to original U.S. Government Works. Distributed under a Creative Commons Attribution NonCommercial License 4.0 (CC BY-NC).

Downloaded from http://advances.sciencemag.org/ on February 3, 2021